Quantification of the effect of site-specific histone acetylation on chromatin remodeling rate

Masatoshi Wakamori[1], Kohki Okabe[2,3,*], Kiyoe Ura[3,4], Takashi Funatsu[2], Masahiro Takinoue[3,5,*], Takashi Umehara[1,3,*]

[1]Laboratory for Epigenetics Drug Discovery, RIKEN Center for Biosystems Dynamics Research, Yokohama, Kanagawa, Japan. [2]Graduate School of Pharmaceutical Sciences, The University of Tokyo, Hongo, Bunkyo-ku, Tokyo. [3]PRESTO, Japan Science and Technology Agency (JST), Kawaguchi, Saitama, Japan. [4]Graduate School of Science, Chiba University. [5]Department of Computer Science, Tokyo Institute of Technology, Yokohama, Kanagawa, Japan.

*Correspondence and requests for materials should be addressed to K.O. (email: okabe@mol.f.u-tokyo.ac.jp), M.T. (email: takinoue@c.titech.ac.jp) or T.U. (email: takashi.umehara@riken.jp).

Abstract

Eukaryotic transcription is epigenetically regulated by chromatin structure and post-translational modifications (PTMs). For example, lysine acetylation in histone H4 is correlated with activation of RNA polymerase I-, II-, and III-driven transcription from chromatin templates, which requires prior chromatin remodeling. However, quantitative understanding of the contribution of particular PTM states to the sequential steps of eukaryotic transcription has been hampered partially because reconstitution of a chromatin template with designed PTMs is difficult. In this study, we reconstituted a di-nucleosome with site-specifically acetylated or unmodified histone H4, which contained two copies of the *Xenopus* somatic 5S rRNA gene with addition of a unique sequence detectable by hybridization-assisted fluorescence correlation spectroscopy. Using a *Xenopus* oocyte nuclear extract, we analyzed the time course of accumulation of nascent 5S rRNA transcripts generated on chromatin templates *in vitro*. Our mathematical model and fitting analyses revealed that tetra-acetylation of histone H4 at K5/K8/K12/K16 increases the chromatin remodeling rate ~3-fold in comparison with the absence of acetylation. We provide a mathematical model for quantitative evaluation of the contribution of epigenetic modifications to chromatin transcription.

Keywords: chromatin, epigenetics, FCS, genetic code expansion, *Xenopus laevis*.

Eukaryotic genes are transcribed by three classes of multisubunit DNA-dependent RNA polymerases (RNAPs)[1]. Ribosomal RNA (rRNA) genes, protein-coding genes, and short non-coding genes, including those for 5S rRNA and transfer RNA (tRNA), are transcribed by RNAP I, II, and III, respectively[2-4]. Because eukaryotic genomic DNA interacts with positively charged histone proteins and is compacted into chromatin, gene transcription is regulated not only by processes involving a naked DNA template—such as the recruitment of general transcription factors and RNAPs to the promoter, initiation, and elongation—but also by processes involving a chromatin template, such as chromatin accessibility for the transcription machinery and chromatin remodeling[5,6]. The structural unit of chromatin, the nucleosome, is formed by wrapping DNA (145–147 bp) around the histone octamer, which consists of two copies of each of the core histones (H2A, H2B, H3, and H4)[7,8]. Each core histone has a lysine (K)-rich N-terminal tail that protrudes through nucleosomal DNA, and these lysine residues are subjected to post-translational modifications (PTMs) such as acetylation, methylation, and ubiquitination[9]. Lysine acetylation (Kac) of the histone H4 tail facilitates chromatin transcription by RNAPs I, II, and III in comparison with unmodified histone H4[10-16]; this presumably occurs by enhancing the remodeling or repositioning (or both) of the nucleosome positioned near the transcription start site[17,18].

The N-terminal tail of histone H4 has four major acetylation sites (K5, K8, K12, and K16), which are highly conserved from yeast to human. These lysines can be acetylated by histone acetyltransferases, and the number of acetylated residues correlates with RNA transcription activity[15,16,19]. Among several H4 acetylation states[20-23], tetra-acetylation at K5/K8/K12/K16 is particularly important, because this hyperacetylated state is found in euchromatin regions where the nearby genes are transcriptionally most active[24]. H4 acetylation at K5/K8/K12/K16 correlates with the expression of both the RNAP II- and III-transcribed genes[15,16]. However, the contribution of each modification state of each histone to the sequential steps of chromatin transcription is yet to be quantified because of the difficulty in precise reconstitution of a chromatin template with the epigenetic modification(s) of interest[25]. Using genetic code expansion and cell-free protein synthesis, we synthesized histone H4 containing designed site-specific acetylation(s) and reconstituted a H4-K5/K8/K12/K16-tetra-acetylated nucleosome[26,27]. Despite the suggested importance of tetra-acetylation at K5/K8/K12/K16, this modification does not affect the crystal structure of the nucleosome core particle[27]. Therefore, the effect of histone H4 acetylation on the dynamics of the nucleosome core needs to be analyzed.

Because the 5S rRNA gene can be chromatinized with a single nucleosome, it has been used as a model gene in an *in vitro* chromatin transcription assay[28,29]. When whole histones including the H4 tail are acetylated in a di-nucleosome chromatin template containing a tandem of two 5S rRNA gene cassettes (*i.e.* X5S197-2[28]), 5S rRNA transcription is activated *in vitro*[28]. However, it is difficult to monitor transcription in real time because *in vitro* transcripts are usually detected by electrophoresis using radioisotope-labeled UTP.

In this study, we developed a di-nucleosome tandem *Xenopus* 5S rRNA gene cassette with a unique sequence derived from c-*fos*. Hybridization of nascent transcripts containing this sequence with the corresponding antisense fluorescent probe enabled real-time monitoring of transcript accumulation in a *Xenopus* oocyte nuclear extract by fluorescence correlation spectroscopy (FCS). We reconstituted the di-nucleosome chromatin template with non-acetylated or tetra-acetylated histone H4 and monitored accumulation of 5S transcripts. Mathematical modeling allowed us to determine the rates of chromatin remodeling from non-acetylated and H4-tetra-acetylated chromatin templates. The methodology developed in this study can be used for quantitative analysis of the contribution of epigenetic modification(s) to chromatin transcription.

Results

Scheme of chromatin transcription, transcript detection, and modeling. The reconstituted RNAP III-driven chromatin transcription system used is shown in Fig. 1. For analyzing the essential dynamics of chromatin transcription, we postulated four steps on the basis of published data, each representing a chromatin state or reaction: (1) chromatin accessibility, (2) chromatin remodeling, (3) priming before transcription, and (4) 5S rRNA transcription.

Chromatin accessibility (1) for *trans*-acting factors can be evaluated by using enzymes that act on DNA, such as micrococcal nuclease (MNase), DNase I, or transposase[30]. Chromatin remodeling factors or histone chaperones, or both, may access the chromatin template at different rates, depending on the presence or absence of histone acetylation. Chromatin remodeling (2) includes remodeling or repositioning (or both) of the nucleosome around the transcription start site. Chromatin remodeling factors such as RSC (remodel the structure of chromatin), or histone chaperones such as FACT (facilitates chromatin transcription), or both, allow access of *trans*-acting factors (*e.g.*, transcriptional machinery) to DNA through relocation of the nucleosome at the transcription start site, which is observed in both RNAP II and III-transcribed genes[31-33]. The extent to which a certain histone acetylation state facilitates chromatin remodeling and nucleosome repositioning remains unclear[28,34,35]. Priming before transcription (3) includes sequential assembly of the transcription preinitiation complex of general transcription factors TFIIIA/TFIIIB/TFIIIC and RNAP III at the promoter[36-39]. Finally, 5S rRNA is transcribed by RNAP III (4). During RNAP III-dependent transcription elongation, the histone core is moving from a position on the DNA template ahead of RNAP III to a position behind it[40-42]. Single nascent transcripts hybridizing with a fluorescent RNA probe can be counted in real time by FCS microscopy. Using the above literature-based chromatin transcription model, we aimed to establish a mathematical model to quantify the contribution of a certain epigenetic modification state (tetra-acetylation of histone H4 in this study) to chromatin transcription.

Atomic force microscopy (AFM) imaging and micrococcal nuclease (MNase) digestion of the H4-tetra-acetylated di-nucleosome. We reconstituted a di-nucleosome in which two copies of *Xenopus* somatic 5S rRNA gene were connected in tandem (Fig. 2A and Supplementary Fig. 1)[25] and recombinant human histone H4 was either unmodified or tetra-acetylated at K5/K8/K12/K16[26,27]. Site-specific acetylation of histone H4 at K5/K8/K12/K16 was confirmed by Western blotting using specific monoclonal antibodies (Fig. 2B). Histone octamers containing K5/K8/K12/K16-tetra-acetylated H4 (hereafter referred as 4Kac) or unmodified H4 together with bacterially expressed core histones H2A, H2B, and H3[43] were assembled and purified. Using unmodified or 4Kac histone octamers, 5S rRNA gene di-nucleosomes were reconstituted with either the X5S197-2 template DNA (Fig. 2A, top; Supplementary Fig. 1A)[25,28] or the newly designed X5S217F-2 template DNA (Fig. 2A, bottom; Supplementary Fig. 1B); X5S217F-2 had an insertion of a 20-bp human c-*fos*-derived annealing sequence (which is absent in the

Xenopus genome) at the +115 position downstream of the 5S rRNA gene for specific detection of 5S rRNA nascent transcripts.

Using AFM imaging, we found that the unmodified (Fig. 2C) and 4Kac (Fig. 2D) X5S197-2 di-nucleosomes had similar dumbbell-shaped structures. DNA length between the two nucleosome cores did not differ significantly between unmodified di-nucleosomes (41 ± 12 nm; N = 50) and 4Kac di-nucleosomes (44 ± 10 nm; N = 50). We next compared the biochemical accessibilities of micrococcal nuclease (MNase) to the unmodified and 4Kac X5S197-2 di-nucleosomes (Fig. 2E). Toward both di-nucleosomes (424 bp), MNase yielded approximately 145-bp DNA fragments that matched the length of mono-nucleosomal DNA (145–147 bp). The sizes and amounts of this partially digested DNA did not differ between unmodified and 4Kac di-nucleosomes (Fig. 2E), suggesting that they had the same chromatin accessibility. Unmodified and 4Kac di-nucleosomes reconstituted with X5S217F-2 template DNA (Fig. 2F) were used for real-time chromatin transcription assay.

Chromatin transcription and its real-time detection by FCS. The X5S217F-2 di-nucleosomes were transcribed in a *Xenopus* oocyte nuclear extract, which contains RNAP III. An antisense RNA probe (20-nt-long Cy3-labeled 2'-*O*-methyl; 2OMe)[44] was added to this system to bind to the complementary c-*fos*-derived annealing sequence in the nascent 140-nt 5S rRNA transcript (Fig. 3A). Hybridization was assessed in real time at high resolution as an increase in the diffusion time of the fluorescent antisense probe detected by FCS[45-47] (Fig. 3B). When the engineered 5S rRNA is transcribed in the reaction mixture, the diffusion time of the antisense probe, as determined from the fluorescence autocorrelation function (FAF), was extended by sequence-dependent hybridization, whereas 5S rRNA lacking the c-*fos* sequence did not extend the diffusion time of the fluorescent antisense probe (Fig. 3C). For calibration of the transcription level, different concentrations of the engineered 5S rRNA that had been transcribed by T7 RNA polymerase were added to the reaction that contained all components except the DNA template, and we conducted FCS measurements after 10-min incubation. The relationship between the change in log RNA concentration and averaged diffusion time of antisense probe in reaction mixture could be linearly approximated with an excellent fit (correlation coefficient = 0.99; Fig. 3D), confirming that the concentration of nascent transcripts can be quantified by measuring probe diffusion time.

By using a custom-made lid as a cover glass to prevent evaporation, we obtained FAF using as little as 5 µl of the reaction mixtures, thus enabling us to measure the concentrations of nascent transcripts *in vitro* in real time (Fig. 3E). As expected, no RNA synthesis was observed for X5S197-2 naked DNA, which has no probe-annealing sequence, whereas an increase in RNA concentration in a time-dependent manner was observed for X5S217F-2 naked DNA (Fig. 3E). Transcription from the H4-tetra-acetylated di-nucleosome was greater than that from the unmodified di-nucleosome, but both were lower than that from the naked template (Fig. 3E). Hence, these results demonstrate that site-specific acetylation of histone H4 activates chromatin transcription *in vitro*.

Mathematical modeling and analyses of chromatin transcription. To quantify the chromatin transcription kinetics, we constructed a simple mathematical model based on steps (1)–(4) shown in Fig. 1. The definitions of the variables and parameters in our mathematical model explained below are summarized in Supplementary Table 1. First, the concentration of accessible chromatin is expressed by $\alpha_\xi C$, where ξ is the type of chromatin template containing the c-*fos*-derived annealing sequence ('ξ' = '4Kac' for H4-tetra-acetylated chromatin DNA or 'unmod' for unmodified chromatin DNA); C (= 300 nM, fixed) is the concentration of the template ('4Kac' and 'unmod'); and α_ξ is accessibility of chromatin 'ξ'. Given $X_\xi(t)$ and $Y_\xi(t)$ are the concentrations of the remodeled chromatin 'ξ' and primed chromatin 'ξ' at time t, respectively, the concentration of chromatin 'ξ' to be remodeled is $(\alpha_\xi C - X_\xi - Y_\xi)$ (Fig. 4A). The chromatin remodeling reaction is described as

$$(\alpha_\xi C - X_\xi - Y_\xi) \overset{k_\xi}{\rightarrow} X_\xi,$$

where k_ξ is the remodeling rate of chromatin 'ξ'. Thus, the priming reaction before transcription is described as

$$X_\xi \overset{k_\mathrm{p}}{\rightarrow} Y_\xi,$$

where k_p is the priming rate of remodeled chromatin 'ξ'. Finally, 5S rRNA transcription reaction is described as follows by assuming the Michaelis–Menten-type enzymatic reaction

$$Y_\xi \xrightarrow{k_\mathrm{cat}, K_\mathrm{m}, C_\mathrm{RP}} Z_\xi,$$

where $Z_\xi(t)$ are the concentrations of the transcribed RNA produced from chromatin 'ξ' at time t; k_cat, K_m, and C_RP are the turnover number, the Michaelis–Menten constant, and the concentration of RNAP III, respectively.

From the chemical reaction model, we have the following ordinary differential equations:

$$\frac{\mathrm{d}X_\xi}{\mathrm{d}t} = k_\xi\left(\alpha_\xi C - X_\xi - Y_\xi\right) - k_\mathrm{p} X_\xi, \tag{1}$$

$$\frac{\mathrm{d}Y_\xi}{\mathrm{d}t} = k_\mathrm{p}\, X_\xi, \tag{2}$$

$$\frac{\mathrm{d}Z_\xi}{\mathrm{d}t} = \frac{k_\mathrm{cat} C_\mathrm{RP} Y_\xi}{K_\mathrm{m} + Y_\xi} \sim \frac{k_\mathrm{cat} C_\mathrm{RP}}{K_\mathrm{m}} Y_\xi, \tag{3}$$

where $K_\mathrm{m} \gg C > Y_\xi$ because K_m for eukaryotic RNA polymerase III is 7 to 83 μM[48] and C in this study was 300 nM. By solving equations (1) – (3) under the initial condition $X_\xi(0) = Y_\xi(0) = Z_\xi(0) = 0$, the kinetics of 5S rRNA transcription from the H4-tetra-acetylated chromatin DNA and the unmodified chromatin DNA is obtained as

$$Z_\xi = \gamma\alpha_\xi \left[t - \left\{ \frac{k_p}{k_\xi (k_\xi - k_p)} e^{-k_\xi t} + \frac{k_\xi + k_p}{k_\xi k_p} - \frac{k_\xi}{k_p (k_\xi - k_p)} e^{-k_p t} \right\} \right], \tag{4}$$

where ξ is '4Kac' or 'unmod'; $\gamma = \frac{k_\mathrm{cat} C_\mathrm{RP}}{K_\mathrm{m}}$ is the transcription rate; the term $\gamma\alpha_\xi t$ means pure transcription without the need for chromatin remodeling or priming; the term $-\left\{ \frac{k_p}{k_\xi (k_\xi - k_p)} e^{-k_\xi t} + \frac{k_\xi + k_p}{k_\xi k_p} - \frac{k_\xi}{k_p (k_\xi - k_p)} e^{-k_p t} \right\}$ indicates the pre-transcription time delay caused by chromatin remodeling and priming (Fig. 4B).

By taking the limit of $k_\xi t \to \infty$, $k_p / k_\xi \to 0$, and $\alpha_\xi = 1$ in equation (4), the kinetics of 5S rRNA transcription from the naked DNA containing the c-*fos*-derived annealing sequence are

$$Z_\mathrm{naked} = \gamma \left[t - \frac{1 - e^{-k_\mathrm{p} t}}{k_\mathrm{p}} \right], \tag{5}$$

where Z_naked are the concentrations of the transcribed RNA produced from 'naked' DNA at time *t* (Fig. 4C).

Using equations (4) and (5), we simulated dynamics of chromatin transcription with different k_4Kac (Fig. 4D) and different α_4Kac (Fig. 4E). It was confirmed that the chromatin remodeling rate k_ξ contributes to the time delay, not to the final slope of the kinetics (Fig. 4D). On the other hand, the accessibility α_ξ contributes to the final slope of the kinetics, not to the time delay (Fig. 4E).

Subsequently, we estimated the kinetic parameters of chromatin transcription by fitting the experimental data to the mathematical model using the computing software Mathematica 11.3 (Wolfram Research, Champaign, IL, USA). First, by fitting the transcription data of the naked DNA to equation (5), the transcription rate γ and the priming rate k_p were determined (Fig. 5A): $\gamma \sim 0.046$ nM min^{-1} and $k_\mathrm{p} \sim 0.13$ min^{-1}. These values were used to estimate the kinetics of transcription from all types of DNA templates. Next, assuming $\alpha_{\mathrm{4Kac}} = \alpha_{\mathrm{unmod}} = 1$, fitting the 5S rRNA transcription data of the H4-tetra-acetylated and unmodified chromatin DNA to equation (4) (Fig. 5B) resulted in the chromatin remodeling rates $k_{\mathrm{4Kac}} \sim 0.12$ min^{-1} and $k_{\mathrm{unmod}} \sim 0.039$ min^{-1}. Because all coefficients of determination, R^2, were sufficiently large (>0.93), the fitting was considered to have been performed properly (Fig. 5A and 5B). This suggests that the mathematical model constructed here can express the transcriptional dynamics. In addition, to examine the adequacy of the assumption of $\alpha_{\mathrm{4Kac}} = \alpha_{\mathrm{unmod}} = 1$, we fitted the data for $\alpha_{\mathrm{unmod}} = 0.8 - 1$ (Supplementary Fig. 2). Because the k_{unmod} and R^2 values did not change much even when α_{unmod} was changed, the simplest assumption of $\alpha_{\mathrm{4Kac}} = \alpha_{\mathrm{unmod}} = 1$ was adopted on the basis of the results of MNase digestion assays (Fig. 2E). Thus, the mathematical analysis shows the remodeling rate of H4-tetra-acetylated chromatin DNA to be approximately 3-fold that of unmodified chromatin DNA (k_{4Kac} / $k_{\mathrm{unmod}} \sim 3.1$) (Fig. 5C).

Discussion

Although it has been known since the 1960s that acetylation of N-terminal tails of core histones facilitates chromatin transcription[10,49], the contribution of each histone modification state has not been quantified. In this study, we have developed a methodology for such quantification by a fluorescence-based transcription tracking method in a reconstituted system and mathematical modeling.

To understand the role of a particular epigenetic modification, a protein with this modification has to be produced, for example by enzymatic modification[50], native chemical ligation[51], or genetic code expansion[52,53]. To produce H4 histone with four sites specifically acetylated, we combined genetic code expansion and cell-free protein synthesis, but other methods may also be used. By comparing RNAP III-driven transcription dynamics in unmodified and H4-tetra-acetylated di-nucleosomes containing 5S rRNA gene cassettes, we established a platform to evaluate the rates of transcription and chromatin remodeling. In this assay, the increase in chromatin remodeling rate by H4 tetra-acetylation was approximately 3-fold (k_{4Kac} / k_{unmod} ~ 3.1). This rate may be further increased by site-specific acetylation of other core histone subunits[15]. Because the methodology developed here is versatile, the roles of other histone PTMs (such as methylation and ubiquitination) can also be quantified. The model may also be used for RNAP II-driven chromatin transcription, chromatin DNA replication, and other aspects of DNA metabolism.

Real-time measurement of transcription in crude extracts is challenging because the absolute amount of the reconstituted chromatin template is usually small, which makes conventional measurements in a cuvette difficult. In this study, we overcame this problem by using a fluorescent probe with high affinity and specificity, and highly sensitive detection by FCS. Measurements of molecular diffusion by FCS reduces the likelihood of obtaining false positives, which is a problem when solely detecting a change in fluorescence. Furthermore, FCS, based on single molecule counting, enables detection of RNA newly synthesized from a very small amount of template. We found that minimization of the reaction volume (*e.g.*, less than 5 μl) and extension of the measurement time (*e.g.*, more than 20 min) are technical bottlenecks caused by evaporation of the reaction solution during the measurement. Considering the femtoliter order of the FCS measurement region, much smaller volumes and longer measurements can be achieved by integration with microfluidic device technologies. By using the developed transcription tracking method in a reconstituted system, the effects of chemical factors (*e.g.*, other PTMs, ions, pH) and physical factors (*e.g.*, temperature, viscosity, congestion) on the dynamics of chromatin transcription can be investigated. Considering the highly quantitative nature of FCS and the requirement for just a few-microliter reaction volume, the present methodology may also be applicable to a living cell[47].

Our mathematical model quantitatively describes the chromatin remodeling step of eukaryotic chromatin transcription although it does not explicitly describe nucleosome positioning and preinitiation complex formation. We obtained the chromatin remodeling rates k_{4Kac} and k_{unmod} and confirmed the validity of data fitting, as judged from their biochemically reasonable values. The remodeling rate of H4-tetra-acetylated chromatin was approximately 3 times that of unmodified chromatin. This finding is important for characterization of the effect of this modification: despite little structural difference from unmodified chromatin, H4-tetra-acetylated chromatin showed considerably more active dynamics of transcription. The effect of the difference in chromatin remodeling rates observed in this study will be clearer when our methodology is applied to living cells or other PTMs.

The constructed mathematical model [equation (4)] provides insights into chromatin transcription. When focusing on a very short-term process ($k_\xi t \ll 1$), $Z_\xi \to \frac{1}{6}\gamma\beta_\xi t^3$, where $\beta_\xi = \alpha_\xi k_\mathrm{p} k_\xi$ (min^{-2}); $\left(k_\mathrm{cat}\beta_\xi\right)^{\frac{1}{3}}$ (min^{-1}) is an apparent initial rate of chromatin transcription. If very short-term transcription kinetics are quantitatively measured, β_ξ or $\left(k_\mathrm{cat}\beta_\xi\right)^{\frac{1}{3}}$ can be used for classifying chromatin transcription in various epigenetic modification states. When focusing on a long-term process ($k_\xi t \gg 1, k_\mathrm{p} t \gg 1$), $Z_\xi \to \gamma\alpha_\xi t$; thus, by measuring the slope of chromatin transcription, chromatin accessibility can be determined more precisely, although in this study it was assumed to be 1 on the basis of the results of MNase digestion assays.

In summary, we established an *in vitro* reconstitution system to quantify the contribution of a certain epigenetic modification state to chromatin transcription dynamics. As a model case, we compared the kinetics of chromatin remodeling and transcription between unmodified and H4-tetra-acetylated chromatin templates. Chromatin templates with certain PTMs, such as site-specific acetylation, can be used in crude extracts in which the product molecules of interest can be counted in real time. Therefore, our methodology will be applicable to a wide variety of chromatin-mediated reactions for quantitative understanding of the importance of epigenetic modifications.

Methods

Reconstitution of H4-acetylated histone octamers. Core histones were prepared and histone octamers were refolded essentially as described previously[54]. Briefly, the fulllength human histones H2A type 1-B/E, H2B type 1-J, and H3.1 were produced in *E. coli* BL21 (DE3) and purified by Ni-Sepharose affinity chromatography. K5/K8/K12/K16-acetylated histone H4 was produced in an *E. coli* cell-free protein synthesis system with the expanded genetic code[26] as described in [27]. For refolding of histone octamers, equimolar amounts of histones (*i.e.*, H2A, H2B, H3, and unmodified or tetra-acetylated H4) were dissolved in 20 mM Tris-HCl buffer (pH 7.5) containing 6 M guanidine-HCl and 10 mM DTT, and dialyzed against 10 mM Tris-HCl buffer (pH 7.5) containing 2 M NaCl, 1 mM EDTA, and 5 mM 2-mercaptoethanol. The histone octamers were purified by size-exclusion chromatography on a Superdex 200 column (GE Healthcare).

Preparation of di-nucleosome DNA. The 424-bp di-nucleosome DNA fragment X5S197-2 composed of two tandem cassettes of the 197-bp *Xenopus borealis* somatic 5S rRNA gene with an upstream sequence (Fig. 2A, top) was prepared as previously described[25]. To produce the 479-bp di-nucleosome DNA fragment (X5S217F-2; Fig. 2A, bottom), two synthetic DNAs (250 bp and 229 bp) were purchased from Eurofins Genomics. The 250-bp DNA was the first 5S rRNA gene cassette (–108 to +142), in which a *Pvu*II site (5'-CAGCTG-3') was inserted at the 5' end and the c-*fos* antisense probe sequence (5'-GCGGA GACAG ACCAA CTAGA-3') was inserted at the +115 position. The 229-bp DNA was the second 5S rRNA gene cassette (–77 to +152), in which the c-*fos* antisense probe sequence was inserted at the +115 position and the *Pvu*II site was inserted at the 3' end. The two DNAs were ligated using a Gibson Assembly Master Mix (New England Biolabs) and subcloned into the pWMD01 vector[55]. The di-nucleosome DNA with the modified 5S rRNA gene cassettes (X5S217F-2) was excised with *Pvu*II and purified by ion-exchange chromatography on a TSK-gel DEAE-5PW column (Tosoh Corporation).

Reconstitution of di-nucleosome chromatin templates. Di-nucleosomes with or without histone H4 acetylation were reconstituted by salt dialysis[25]. Briefly, purified histone octamers were mixed with the X5S197-2 or X5S217F-2 fragment DNA in 10 mM Tris-HCl buffer (pH 7.5) containing 2 M NaCl, 1 mM EDTA, and 1 mM 2-mercaptoethanol (histone octamer: DNA = 0.9 : 1.0 w/w), and dialyzed at 4 °C for 16 h. Then, stepwise dialysis was performed against buffers with decreasing NaCl concentrations. The reconstituted di-nucleosomes were fractionated by centrifugation in 10%–25% sucrose gradients at 36,000 rpm at 4 °C for 16 h in a Beckman SW41 rotor. Forty fractions were collected using a Piston Gradient Fractionator (BioComp) and electrophoresed in 0.5× TBE buffer at 8.5 V/cm in a 0.7% Seakem GTG agarose gel and visualized by ethidium bromide staining. Di-nucleosomes from the 20th to 22nd fractions were pooled, concentrated using an Amicon Ultra 0.5 ml 10K centrifugal filter, and dialyzed against 10 mM HEPES buffer (pH 7.5) containing 100 µM EDTA; their concentration was determined from the optical density at a wavelength of 260 nm.

Atomic force microscopy. Di-nucleosomes (90 ng/µl) were fixed with 0.1% glutaraldehyde for 16 h at 4 °C. Immediately before measurement, they were diluted to 0.45 ng/µl with 10 mM HEPES buffer (pH 7.5), placed onto APTES-treated mica[56] and left for 10 min. Imaging was performed using a high-speed AFM system (Nano Live Vision, RIBM, Tsukuba, Japan) with a carbon nanofiber cantilever (BL-AC10FS, Olympus) at a spring constant of 0.1 N/m in solution phase at 27 °C. Images of a 500 × 375-nm area were obtained at 2 s/frame at a resolution of 192 × 144 pixels. DNA length between two nucleosome core particles was traced manually in the images and quantified using ImageJ software (version 1.45s).

Micrococcal nuclease digestion. DNA of di-nucleosome (100 ng) containing either tetra-acetylated or unmodified histone H4 was digested for 5 min at 22 °C with MNase (0.125 to 2.0 units; Takara, cat. #2910A) in 5.5 mM Tris-HCl buffer (pH 7.6) containing 500 µM $CaCl_2$ and 50 µg/ml BSA. Digestion was terminated by addition of 20 mM EDTA and 0.5% (w/v) SDS containing 2 µg of proteinase K (Roche, cat. #3115887). DNA fragments were extracted with phenol/chloroform and analyzed by electrophoresis in a non-denaturing 10% polyacrylamide gel.

Transcription *in vitro* and transcript detection by fluorescence correlation spectroscopy. Transcription was performed essentially as described[57]. Each reaction mixture (10 µl) contained purified di-nucleosome or naked DNA template (1 µg) , 0.9 µl of a *Xenopus* oocyte nuclear extract, 9.5 mM HEPES (pH 7.4), 100 mM NaCl, 48 mM KCl, 6.7 mM $MgCl_2$, 3.6 mM DTT, 90 µM EDTA, 4.5% (v/v) glycerol, 0.9% (w/v) polyvinylpyrrolidone, 0.06% (w/v) BSA, 500 µM NTPs, 1 µM trichostatin A, 5 units of RNase inhibitor (Toyobo, cat. #SIN-201), and 20 nM c-*fos* antisense probe. The c-*fos* probe was synthesized with a 2′ O-Me RNA backbone, which was labeled with Cy3 at its 3′ end. FCS was conducted on a confocal laser-scanning fluorescence microscope (TCS SP8, Leica) equipped with a single molecule detection unit (PicoQuant) at 23 °C. The reaction mixture (5 µl) was covered with a stainless-steel cylinder (inner diameter, 6.2 mm; length, 5 mm), one end of which was covered with a cover glass. Cy3 fluorescence was excited with a green laser (532 nm, Leica), and emitted photons were captured through an objective lens (63×, HC PL APO CS2 1.20 N.A. water, Leica) with a 570DF30 emission filter (Omega). Each 30-s fluorescence fluctuation measurement was performed with an avalanche photodiode (PicoQuant). Total recording time was about 20 min. Autocorrelation was calculated with the SymPhoTime software (PicoQuant). The obtained fluorescence autocorrelation between 0.01 and 813 ms was approximated with SymPhoTime using the autocorrelation function [equation (6)] with one component:

$$G(\tau) - 1 = \frac{1}{N} \times \left(\frac{1}{1+\tau/\tau_1}\right)\left(\frac{1}{1+(1/\kappa)^2(\tau/\tau_1)}\right)^{\frac{1}{2}} \tag{6}$$

where N is the number of fluorescent dyes in the confocal volume, τ_1 is the diffusion time, and κ is a structure parameter (10–15 in this experiment).

Author contributions

M.W., K.O., M.T., and T.U. designed the experiments, interpreted the results, and wrote the manuscript. M.W., K.U., and T.U. performed the biochemical analysis. K.O. and T.F. performed the biophysical analysis. M.T. performed the mathematical analysis. All authors commented on the manuscript.

Acknowledgments

We thank Hiroki R. Ueda (the University of Tokyo) for encouragement, Toshiaki Higo for sample preparation, and Yuki Saito for clerical assistance. This work was supported by grants from the PRESTO program of the Japan Science and Technology Agency (JST), and in part by Grants-in-Aid for Scientific Research on Innovative Areas to K.O. (No. 15H05931) and K.U. (No. 15H01345), a Grant-in-Aid for Challenging Research (Exploratory) to M.T. (No. 18K19834), and Grants-in-Aid for Scientific Research (B) to

M.T. (No. 17H01813) and T.U. (No. 16H05089) from the Japan Society for the Promotion of Science (JSPS).

References

1 Roeder, R. G. & Rutter, W. J. Multiple forms of DNA-dependent RNA polymerase in eukaryotic organisms. *Nature* **224**, 234-237 (1969).
2 Dignam, J. D., Lebovitz, R. M. & Roeder, R. G. Accurate transcription initiation by RNA polymerase II in a soluble extract from isolated mammalian nuclei. *Nucleic acids research* **11**, 1475-1489 (1983).
3 Keener, J., Josaitis, C. A., Dodd, J. A. & Nomura, M. Reconstitution of yeast RNA polymerase I transcription in vitro from purified components. TATA-binding protein is not required for basal transcription. *The Journal of biological chemistry* **273**, 33795-33802 (1998).
4 Vannini, A. & Cramer, P. Conservation between the RNA polymerase I, II, and III transcription initiation machineries. *Molecular cell* **45**, 439-446, doi:10.1016/j.molcel.2012.01.023 (2012).
5 Paranjape, S. M., Kamakaka, R. T. & Kadonaga, J. T. Role of chromatin structure in the regulation of transcription by RNA polymerase II. *Annual review of biochemistry* **63**, 265-297 (1994).
6 Felsenfeld, G. Chromatin as an essential part of the transcriptional mechanism. *Nature* **355**, 219, doi:10.1038/355219a0 (1992).
7 Luger, K., Mader, A. W., Richmond, R. K., Sargent, D. F. & Richmond, T. J. Crystal structure of the nucleosome core particle at 2.8 A resolution. *Nature* **389**, 251-260, doi:10.1038/38444 (1997).
8 Kornberg, R. D. & Lorch, Y. L. Twenty-five years of the nucleosome, fundamental particle of the eukaryote chromosome. *Cell* **98**, 285-294, doi:10.1016/S0092-8674(00)81958-3 (1999).
9 Peterson, C. L. & Laniel, M.-A. Histones and histone modifications. *Current Biology* **14**, R546-R551, doi:10.1016/j.cub.2004.07.007 (2004).
10 Allfrey, V. G., Faulkner, R. & Mirsky, A. E. Acetylation and Methylation of Histones and Their Possible Role in the Regulation of RNA Synthesis. *Proceedings of the National Academy of Sciences of the United States of America* **51**, 786-794 (1964).
11 Lee, D. Y., Hayes, J. J., Pruss, D. & Wolffe, A. P. A positive role for histone acetylation in transcription factor access to nucleosomal DNA. *Cell* **72**, 73-84 (1993).
12 Hirschler-Laszkiewicz, I. *et al.* The role of acetylation in rDNA transcription. *Nucleic acids research* **29**, 4114-4124 (2001).
13 Eberharter, A. & Becker, P. B. Histone acetylation: a switch between repressive and permissive chromatin. *Second in review series on chromatin dynamics* **3**, 224-229, doi:10.1093/embo-reports/kvf053 (2002).
14 Grummt, I. & Pikaard, C. S. Epigenetic silencing of RNA polymerase I transcription. *Nature reviews. Molecular cell biology* **4**, 641-649, doi:10.1038/nrm1171 (2003).
15 Barski, A. *et al.* Pol II and its associated epigenetic marks are present at Pol III–transcribed noncoding RNA genes. *Nature structural & molecular biology* **17**, 629 (2010).
16 White, R. J. Transcription by RNA polymerase III: more complex than we thought. *Nature reviews. Genetics* **12**, 459-463, doi:10.1038/nrg3001 (2011).
17 Wolffe, A. P. Nucleosome positioning and modification: chromatin structures that potentiate transcription. *Trends in biochemical sciences* **19**, 240-244 (1994).
18 Jiang, C. & Pugh, B. F. Nucleosome positioning and gene regulation: advances through genomics. *Nature Reviews Genetics* **10**, 161, doi:10.1038/nrg2522 (2009).

19 Turner, B. M. Histone acetylation and control of gene expression. *Journal of cell science* **99**, 13-20 (1991).

20 Zhang, K. *et al.* Histone Acetylation and Deacetylation. *Identification of Acetylation and Methylation Sites of HeLa Histone H4 by Mass Spectrometry* **1**, 500-508, doi:10.1074/mcp.M200031-MCP200 (2002).

21 Smith, C. M. *et al.* Mass spectrometric quantification of acetylation at specific lysines within the amino-terminal tail of histone H4. *Analytical biochemistry* **316**, 23-33, doi:10.1016/S0003-2697(03)00032-0 (2003).

22 Wang, C. I. *et al.* ChIP-mass spectrometry captures protein interactions and modified histones associated with dosage compensation in Drosophila. *Nature structural & molecular biology* **20**, 202-209, doi:10.1038/nsmb.2477 (2013).

23 Henry, R. A. *et al.* Quantitative measurement of histone tail acetylation reveals stage-specific regulation and response to environmental changes during Drosophila development. *Biochemistry-Us* **55**, 1663-1672, doi:10.1021/acs.biochem.5b01070 (2016).

24 Grunstein, M. Histone acetylation in chromatin structure and transcription. *Nature* **389**, 349, doi:10.1038/38664 (1997).

25 Ura, K., Hayes, J. J. & Wolffe, A. P. A positive role for nucleosome mobility in the transcriptional activity of chromatin templates: restriction by linker histones. *The EMBO journal* **14**, 3752-3765 (1995).

26 Mukai, T. *et al.* Genetic-code evolution for protein synthesis with non-natural amino acids. *Biochemical and biophysical research communications* **411**, 757-761, doi:10.1016/J.Bbrc.2011.07.020 (2011).

27 Wakamori, M. *et al.* Intra- and inter-nucleosomal interactions of the histone H4 tail revealed with a human nucleosome core particle with genetically-incorporated H4 tetra-acetylation. *Scientific reports* **5**, 17204, doi:10.1038/srep17204 (2015).

28 Ura, K., Kurumizaka, H., Dimitrov, S., Almouzni, G. & Wolffe, A. P. Histone acetylation: influence on transcription, nucleosome mobility and positioning, and linker histone-dependent transcriptional repression. *The EMBO journal* **16**, 2096-2107, doi:10.1093/emboj/16.8.2096 (1997).

29 Tse, C., Sera, T., Wolffe, A. P. & Hansen, J. C. Disruption of higher-order folding by core histone acetylation dramatically enhances transcription of nucleosomal arrays by RNA polymerase III. *Mol Cell Biol* **18**, 4629-4638 (1998).

30 Tsompana, M. & Buck, M. J. Chromatin accessibility: a window into the genome. *Epigenetics & chromatin* **7**, 33, doi:10.1186/1756-8935-7-33 (2014).

31 Birch, J. L. *et al.* FACT facilitates chromatin transcription by RNA polymerases I and III. *The EMBO journal* **28**, 854-865, doi:10.1038/emboj.2009.33 (2009).

32 Helbo, A. S., Lay, F. D., Jones, P. A., Liang, G. & Gronbaek, K. Nucleosome Positioning and NDR Structure at RNA Polymerase III Promoters. *Scientific reports* **7**, 41947, doi:10.1038/srep41947 (2017).

33 Parnell, T. J., Huff, J. T. & Cairns, B. R. RSC regulates nucleosome positioning at Pol II genes and density at Pol III genes. *The EMBO journal* **27**, 100-110, doi:10.1038/sj.emboj.7601946 (2008).

34 Bresnick, E. H., John, S. & Hager, G. L. Histone hyperacetylation does not alter the positioning or stability of phased nucleosomes on the mouse mammary tumor virus long terminal repeat. *Biochemistry-Us* **30**, 3490-3497 (1991).

35 Eberharter, A. & Becker, P. B. Histone acetylation: a switch between repressive and permissive chromatin. Second in review series on chromatin dynamics. *EMBO reports* **3**, 224-229, doi:10.1093/embo-reports/kvf053 (2002).

36 Dieci, G., Fiorino, G., Castelnuovo, M., Teichmann, M. & Pagano, A. The expanding RNA polymerase III transcriptome. *Trends in Genetics* **23**, 614-622, doi:10.1016/j.tig.2007.09.001 (2007).

37 Orioli, A., Pascali, C., Pagano, A., Teichmann, M. & Dieci, G. RNA polymerase III transcription control elements: Themes and variations. *Gene* **493**, 185-194, doi:10.1016/j.gene.2011.06.015 (2012).

38 Arimbasseri, A. G., Rijal, K. & Maraia, R. J. Comparative overview of RNA polymerase II and III transcription cycles, with focus on RNA polymerase III termination and reinitiation. *Transcription* **5**, e27639, doi:10.4161/trns.27369 (2014).

39 Leśniewska, E. & Boguta, M. Novel layers of RNA polymerase III control affecting tRNA gene transcription in eukaryotes. *Open biology* **7**, 170001, doi:10.1098/rsob.170001 (2017).

40 Clark, D. J. & Felsenfeld, G. A nucleosome core is transferred out of the path of a transcribing polymerase. *Cell* **71**, 11-22 (1992).

41 Studitsky, V. M., Kassavetis, G. A., Geiduschek, E. P. & Felsenfeld, G. Mechanism of Transcription Through the Nucleosome by Eukaryotic RNA Polymerase. *Science* **278**, 1960-1963, doi:10.1126/science.278.5345.1960 (1997).

42 Workman, J. L. Nucleosome displacement in transcription. *Genes & development* **20**, 2009-2017, doi:10.1101/gad.1435706 (2006).

43 Dyer, P. N. *et al.* Reconstitution of nucleosome core particles from recombinant histones and DNA. *Methods in enzymology* **375**, 23-44 (2004).

44 Okabe, K. *et al.* Real time monitoring of endogenous cytoplasmic mRNA using linear antisense 2′ -O-methyl RNA probes in living cells. *Nucleic acids research* **39**, e20-e20, doi:10.1093/nar/gkq1196 (2011).

45 Kettling, U., Koltermann, A., Schwille, P. & Eigen, M. Real-time enzyme kinetics monitored by dual-color fluorescence cross-correlation spectroscopy. *Proceedings of the National Academy of Sciences* **95**, 1416-1420, doi:10.1073/pnas.95.4.1416 (1998).

46 Medina, M. Á. & Schwille, P. Fluorescence correlation spectroscopy for the detection and study of single molecules in biology. *Bioessays* **24**, 758-764, doi:doi:10.1002/bies.10118 (2002).

47 Zhang, J., Okabe, K., Tani, T. & Funatsu, T. Dynamic association-dissociation and harboring of endogenous mRNAs in stress granules. *Journal of cell science* **124**, 4087-4095, doi:10.1242/jcs.090951 (2011).

48 Szafranski, P. & Smagowicz, W. J. Relative affinities of nucleotide substrates for the yeast tRNA gene transcription complex. *Zeitschrift fur Naturforschung. C, Journal of biosciences* **47**, 320-321 (1992).

49 Verdin, E. & Ott, M. 50 years of protein acetylation: from gene regulation to epigenetics, metabolism and beyond. *Nature reviews. Molecular cell biology* **16**, 258-264, doi:10.1038/nrm3931 (2015).

50 Mishima, Y. *et al.* Hinge and chromoshadow of HP1alpha participate in recognition of K9 methylated histone H3 in nucleosomes. *Journal of molecular biology* **425**, 54-70, doi:10.1016/j.jmb.2012.10.018 (2013).

51 Fierz, B. & Muir, T. W. Chromatin as an expansive canvas for chemical biology. *Nat Chem Biol* **8**, 417-427, doi:10.1038/nchembio.938 (2012).

52 Yanagisawa, T., Umehara, T., Sakamoto, K. & Yokoyama, S. Expanded genetic code technologies for incorporating modified lysine at multiple sites. *Chembiochem : a European journal of chemical biology* **15**, 2181-2187, doi:10.1002/cbic.201402266 (2014).

53 Chin, J. W. Expanding and reprogramming the genetic code. *Nature* **550**, 53-60, doi:10.1038/nature24031 (2017).

54 Tanaka, Y. *et al.* Expression and purification of recombinant human histones. *Methods* **33**, 3-11, doi:10.1016/j.ymeth.2003.10.024 (2004).

55 Wakamori, M., Umehara, T. & Yokoyama, S. A tandem insertion vector for large-scale preparation of nucleosomal DNA. *Analytical biochemistry* **423**, 184-186, doi:10.1016/j.ab.2012.01.010 (2012).

56 Wang, H. *et al.* Glutaraldehyde Modified Mica: A New Surface for Atomic Force Microscopy of Chromatin. *Biophysical journal* **83**, 3619-3625, doi:10.1016/S0006-3495(02)75362-9 (2002).

57 Birkenmeier, E. H., Brown, D. D. & Jordan, E. A nuclear extract of Xenopus laevis oocytes that accurately transcribes 5S RNA genes. *Cell* **15**, 1077-1086 (1978).

Figure Legends

Figure 1. Schematic diagram of 5S rRNA chromatin transcription and its real-time detection.

Figure 2. Reconstitution of H4-tetra-acetylated di-nucleosomes for chromatin transcription. (A) Scheme of di-nucleosome rRNA gene cassettes. Internal control regions (box A; IE, intermediate element; box C) of the 5S rRNA gene are indicated. The X5S197-2 construct[28] (top) was modified by introducing a c-*fos* probe sequence (bottom) for fluorescence correlation spectroscopy measurements. (B) Western blotting of unmodified and site-specifically tetra-acetylated histone H4 proteins. Kac, acetylated lysine. (C, D) Atomic force microscopy images of 5S rRNA di-nucleosomes reconstituted with unmodified histone H4 (C) or K5/K8/K12/K16-acetylated H4 (D). (E) Di-nucleosome digestion with micrococcal nuclease (MNase). Lanes 1, 3, 5, 7 and 9, di-nucleosomes with unmodified H4; lanes 2, 4, 6, 8 and 10, di-nucleosomes with K5/K8/K12/K16-acetylated H4. Lanes 1 and 2, di-nucleosomes were incubated in MNase reaction buffer in the absence of MNase. Units of MNase (Takara, cat. #2910A) per microgram DNA: lanes 3 and 4, 2.5; lanes 5 and 6, 5.0; lanes 7 and 8, 10, lanes 9 and 10, 20. (F) Agarose gel electrophoreses of di-nucleosomes constructed with c-*fos*-derived annealing sequence DNA. Lane M, DNA ladder marker (NEB, cat. N3232S); lane 1, di-nucleosome reconstituted with unmodified H4; lane 2, di-nucleosome reconstituted with K5/K8/K12/K16-tetra-acetylated H4.

Figure 3. Real-time detection of chromatin transcription. (A) Scheme of a Cy3-labeled antisense 2'-*O*-methyl RNA (2OMe-RNA) probe and its hybridization with mRNA. (B)

Scheme of the setup of fluorescence correlation spectroscopy (FCS) for monitoring mRNA synthesis. Changes in diffusion of the antisense probe upon hybridization with transcripts in the confocal volume were detected by an avalanche photodiode (APD) at the single-molecule level. (C) Fluorescence autocorrelation functions [FAF, G(τ)] in reaction solutions. FAF of the antisense probe with mRNA showed longer correlation time than that without mRNA or that of a control probe with mRNA. (Inset) averaged diffusion time of antisense probes. (D) Calibration of the averaged diffusion time of the antisense 5S/c-*fos* RNA probe molecules as a function of their concentration. In (C) and (D), RNA was transcribed by T7 RNA polymerase from two tandem copies of the 5S rRNA gene (Fig. 2A) and added to a *Xenopus* oocyte nuclear extract without template DNA; diffusion time was measured by FCS. Mean ± standard deviation (N = 3). (E) Real-time detection of nascent 5S rRNA transcripts. Template DNAs used are shown in: gray, naked 5S rRNA gene without c-*fos* sequence; black, naked 5S rRNA gene containing the c-*fos*-derived annealing sequence; red, H4-tetra-acetylated di-nucleosome 5S rRNA gene containing c-*fos* sequence; and blue, non-acetylated di-nucleosome 5S rRNA gene containing c-*fos* sequence.

Figure 4. Mathematical model of chromatin transcription. (A) Explanation of modeling of chromatin transcription. Variables are defined in Supplementary Table 1. (B, C) Explanation of the obtained equations. (B) Transcription from chromatin [equation (4)]. (C) Transcription from naked DNA [equation (5)]. (D, E) Numerical simulation of chromatin transcription with different k_{4Kac} (D) and different α_{4Kac} (E). $\gamma = 0.01$ nM min^{-1} and $k_p = 1/15 \approx 0.0667$ min^{-1} are fixed. Z_ξ is the concentration of transcribed RNA, where ξ is '4Kac' or 'naked'. For '4Kac', equation (4) is used, where

k_{4Kac} is changed with $\alpha_{\mathrm{4Kac}} = \alpha_{\mathrm{naked}} = 1$ fixed (D) or α_{4Kac} is changed with $\alpha_{\mathrm{naked}} = 1$ and $k_{\mathrm{4Kac}} = 0.1$ min^{-1} fixed (E). For 'naked', equation (5) is used.

Figure 5. Results of fitting to the mathematical model. (A) Determination of γ and k_p. First, the γ value was determined by fitting the linear region (12–17 min) of the experimental data for the naked DNA (+ c-*fos*) to the mathematical model $Z_{\mathrm{naked}} = \gamma t + z_1$, where z_1 is the intercept; this equation is the long-term limit of equation (5). As a result, γ = 0.046 ± 0.003 nM min^{-1} ('fitting value' ± 'fitting error') (z_1 = –0.29 ± 0.04 nM; coefficient of determination R^2 = 0.998). Then, using the obtained γ, the k_p value was determined by fitting the whole region (0–17 min) of the data to the mathematical model $Z_{\mathrm{naked}} = \gamma\left[\, t - \left(1 - e^{-k_\mathrm{p} t}\right)/k_\mathrm{p} \,\right] + z_2$, where z_2 is the intercept introduced for resolving experimental error at the initial stage [equation (5)]. As a result, k_p = 0.13 ± 0.006 min^{-1} (z_2 = –0.010 ± 0.006 nM; R^2 = 0.993). (B) Fitting results for each condition. Z_ξ is the concentration of transcribed RNA, where ξ is '4Kac', 'unmod', or 'naked' [equations (4) and (5)]. γ = 0.046 nM min^{-1} and k_p = 0.13 min^{-1}, which were obtained in (A), were used for fitting. (C) Schematic illustration of acceleration of chromatin transcription by histone H4 acetylation.

Figure 1

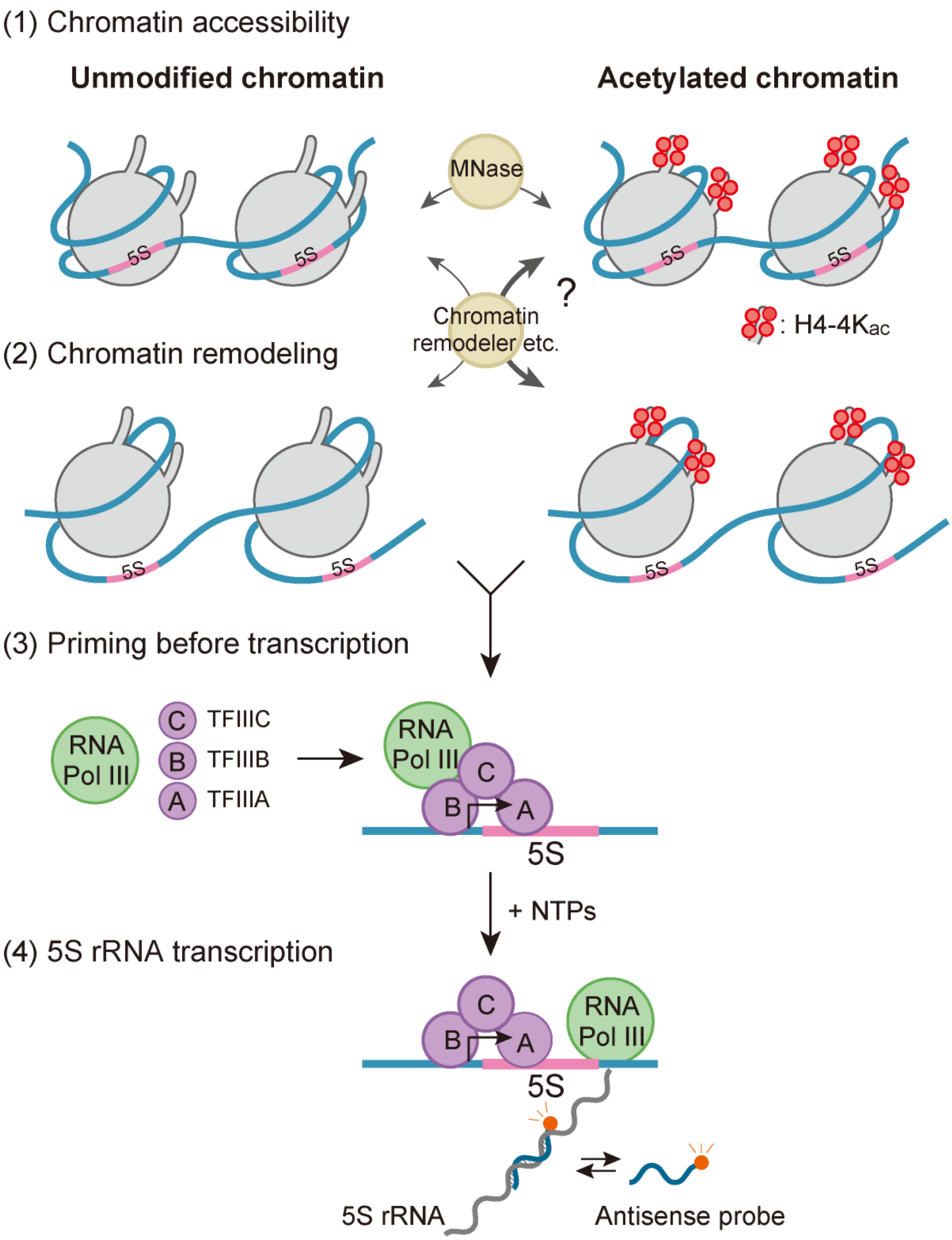
(1) Chromatin accessibility
Unmodified chromatin
Acetylated chromatin
MNase
5S
?
Chromatin remodeler etc.
: H4-4Kac
(2) Chromatin remodeling
(3) Priming before transcription
RNA Pol III
C TFIIIC
B TFIIIB
A TFIIIA
C
B
A
5S
+ NTPs
(4) 5S rRNA transcription
5S rRNA
Antisense probe

Figure 2

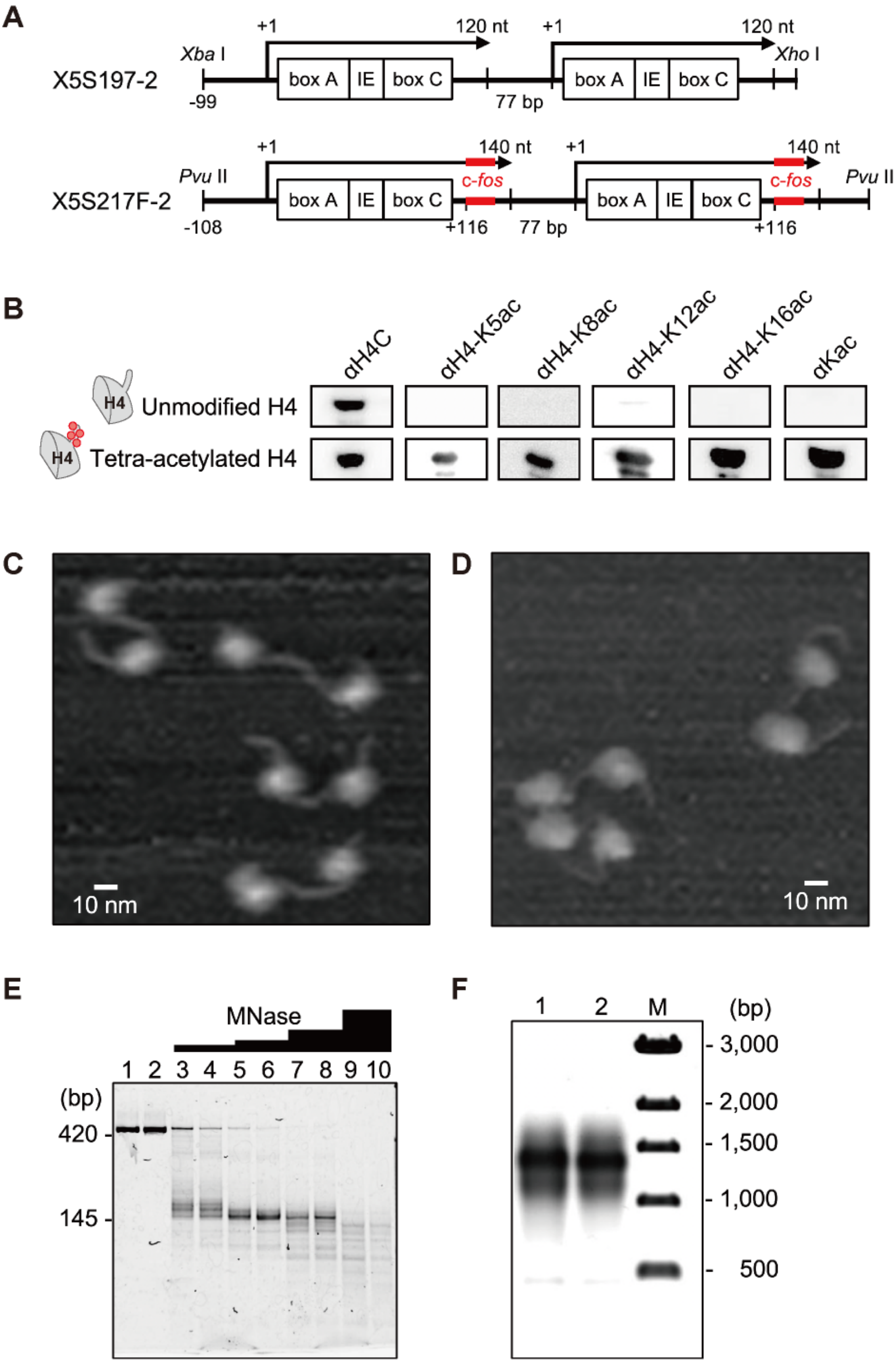
A
X5S197-2
Xba I
-99
+1
120 nt
box A
IE
box C
77 bp
Xho I
X5S217F-2
Pvu II
-108
140 nt
c-fos
+116
B
αH4C
αH4-K5ac
αH4-K8ac
αH4-K12ac
αH4-K16ac
αKac
H4
Unmodified H4
Tetra-acetylated H4
C
D
10 nm
E
MNase
1 2 3 4 5 6 7 8 9 10
(bp)
420
145
F
1 2 M
(bp)
3,000
2,000
1,500
1,000
500

Figure 3

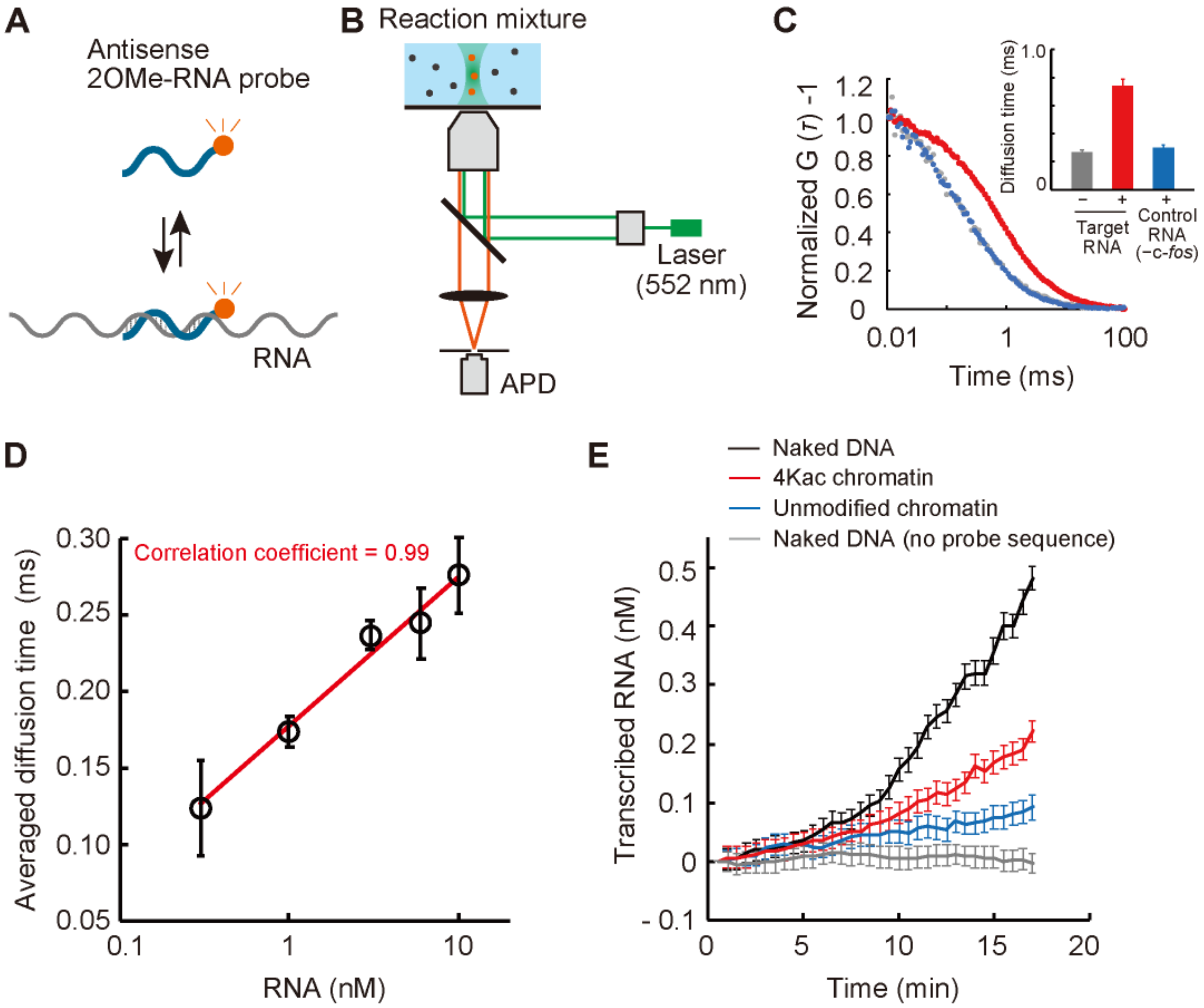
A
Antisense
2OMe-RNA probe
RNA
B Reaction mixture
Laser
(552 nm)
APD
C
Normalized G (τ) -1
Time (ms)
Diffusion time (ms)
Target RNA
Control RNA (−c-fos)
D
Correlation coefficient = 0.99
Averaged diffusion time (ms)
RNA (nM)
E
Naked DNA
4Kac chromatin
Unmodified chromatin
Naked DNA (no probe sequence)
Transcribed RNA (nM)
Time (min)

Figure 4

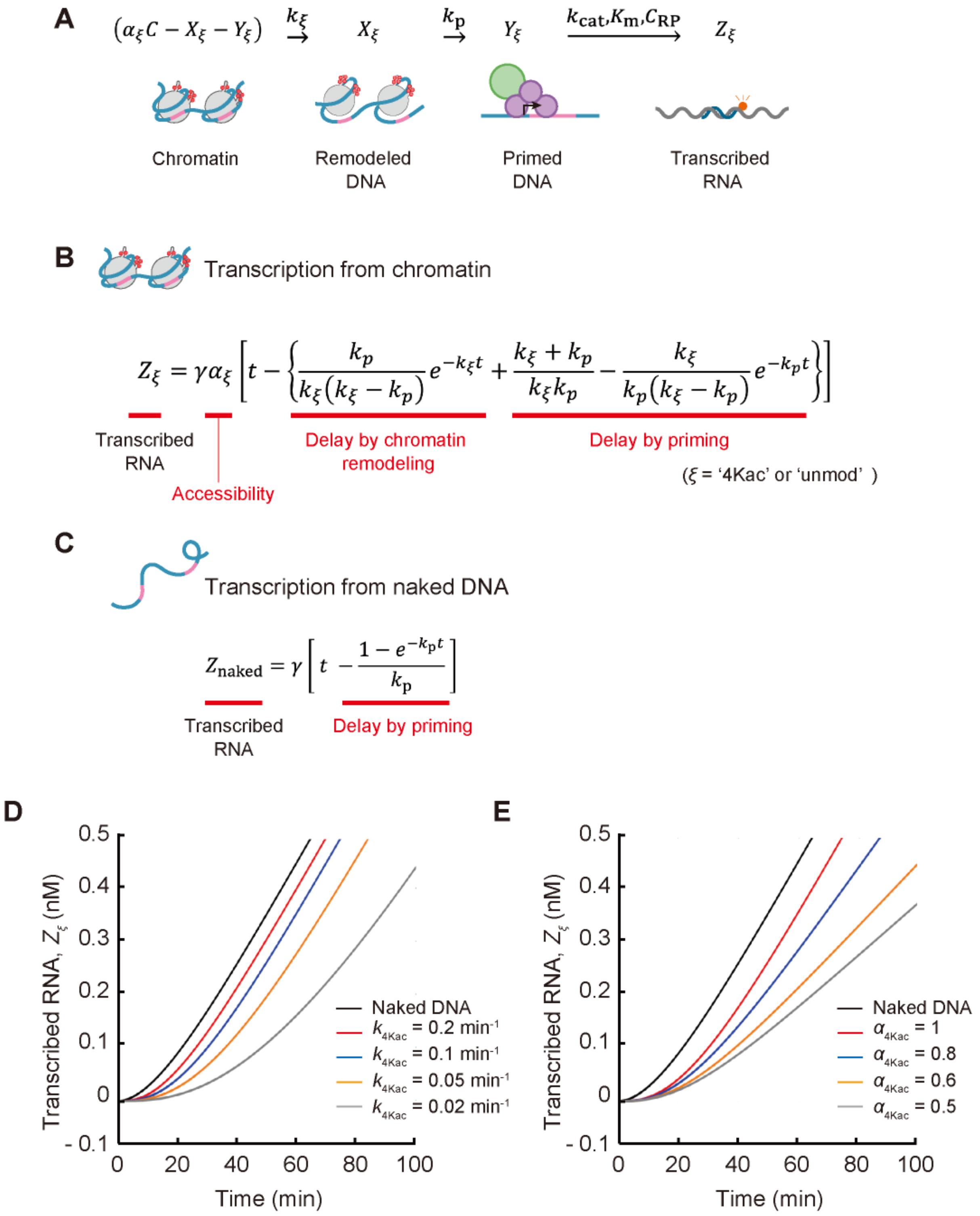
A
$(\alpha_\xi C - X_\xi - Y_\xi) \xrightarrow{k_\xi} X_\xi \xrightarrow{k_p} Y_\xi \xrightarrow{k_{cat}, K_m, C_{RP}} Z_\xi$
Chromatin
Remodeled DNA
Primed DNA
Transcribed RNA
B
Transcription from chromatin
$Z_\xi = \gamma\alpha_\xi \left[t - \left\{ \frac{k_p}{k_\xi(k_\xi - k_p)} e^{-k_\xi t} + \frac{k_\xi + k_p}{k_\xi k_p} - \frac{k_\xi}{k_p(k_\xi - k_p)} e^{-k_p t} \right\} \right]$
Transcribed RNA
Accessibility
Delay by chromatin remodeling
Delay by priming
(ξ = '4Kac' or 'unmod')
C
Transcription from naked DNA
$Z_{naked} = \gamma \left[t - \frac{1 - e^{-k_p t}}{k_p} \right]$
Transcribed RNA
Delay by priming
D
Transcribed RNA, Z_ξ (nM)
Time (min)
Naked DNA
k_{4Kac} = 0.2 min^{-1}
k_{4Kac} = 0.1 min^{-1}
k_{4Kac} = 0.05 min^{-1}
k_{4Kac} = 0.02 min^{-1}
E
Transcribed RNA, Z_ξ (nM)
Time (min)
Naked DNA
α_{4Kac} = 1
α_{4Kac} = 0.8
α_{4Kac} = 0.6
α_{4Kac} = 0.5

Figure 5

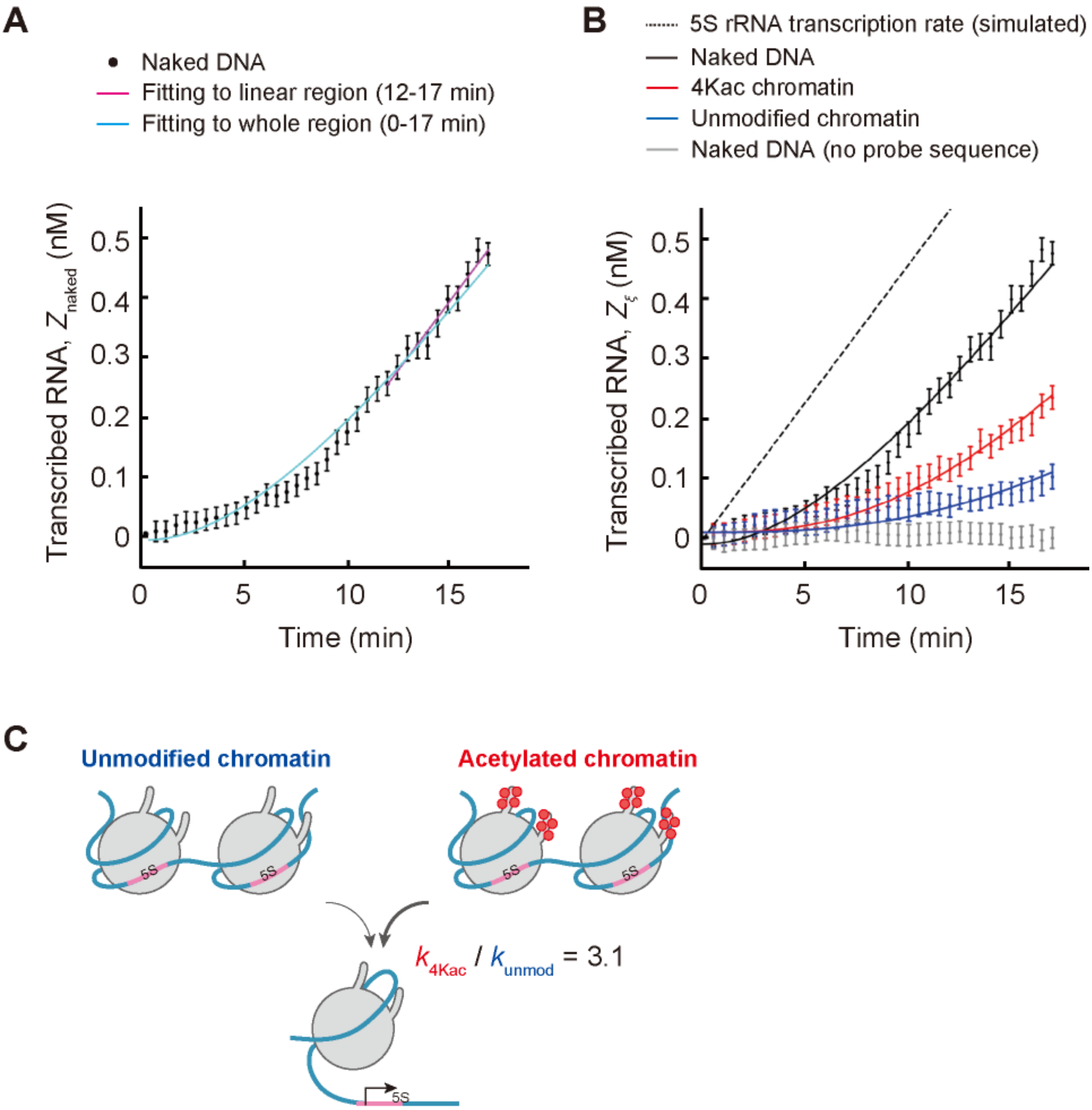
A
Naked DNA
Fitting to linear region (12-17 min)
Fitting to whole region (0-17 min)
Transcribed RNA, Z_{naked} (nM)
Time (min)
B
5S rRNA transcription rate (simulated)
Naked DNA
4Kac chromatin
Unmodified chromatin
Naked DNA (no probe sequence)
Transcribed RNA, Z_ξ (nM)
Time (min)
C
Unmodified chromatin
Acetylated chromatin
5S
k_{4Kac} / k_{unmod} = 3.1